Annu. Rev. Biomed. Eng. 2000. 02:377–97

NEW CURRENTS IN ELECTRICAL STIMULATION OF EXCITABLE TISSUES[1]

Peter J. Basser
Section on Tissue Biophysics & Biomimetics, National Institute of Child Health and Human Development, National Institutes of Health, Bethesda, Maryland 20892-5772; e-mail: pjbasser@helix.nih.gov

Bradley J. Roth
Department of Physics, Oakland University, Rochester, MI 48309-4487; e-mail: roth@oakland.edu

Key Words electric, magnetic, stimulation, bidomain, excitable, nerve, heart, brain

■ **Abstract** Electric fields can stimulate excitable tissue by a number of mechanisms. A uniform long, straight peripheral axon is activated by the gradient of the electric field that is oriented parallel to the fiber axis. Cortical neurons in the brain are excited when the electric field, which is applied along the axon-dendrite axis, reaches a particular threshold value. Cardiac tissue is thought to be depolarized in a uniform electric field by the curved trajectories of its fiber tracts. The bidomain model provides a coherent conceptual framework for analyzing and understanding these apparently disparate phenomena. Concepts such as the activating function and virtual anode and cathode, as well as anode and cathode break and make stimulation, are presented to help explain these excitation events in a unified manner. This modeling approach can also be used to describe the response of excitable tissues to electric fields that arise from charge redistribution (electrical stimulation) and from time-varying magnetic fields (magnetic stimulation) in a self-consistent manner. It has also proved useful to predict the behavior of excitable tissues, to test hypotheses about possible excitation mechanisms, to design novel electrophysiological experiments, and to interpret their findings.

CONTENTS

[1]The US Government has the right to retain a nonexclusive, royalty-free license in and to any copyright covering this paper.

INTRODUCTION

In this review, we describe mechanisms by which electric fields excite electrically active tissues. The mechanism of interaction between the applied electric field and the tissue determines where, when, and how the cell membrane is depolarized or hyperpolarized. Additional information can be found elsewhere (1–5).

Below we distinguish between anodes and cathodes that are "real" (e.g. current or surface electrodes) or "virtual" (i.e. regions of hyperpolarized or depolarized tissue produced by the impressed current and electric field distributions). The terms anode- and cathode-make and anode- and cathode-break stimulation are defined. Anode- or cathode-make stimulation occurs when the anodic or cathodic current is turned on, whereas anode- and cathode-break stimulation occurs when the anodic or cathodic current is turned off. We also use the term "bidomain" below. By that we mean a material that has two distinct but communicating domains, in our case, an "intracellular" and an "extracellular" compartment, which occupy the same point in space.

EXCITATION OF NERVE FIBERS

A single fiber, such as a nerve axon or a muscle fiber, can be used to illustrate several different mechanisms of electrical stimulation. These fibers can be short or long, straight or curved, and uniform or nonuniform. We begin our discussion with the simplest case—the long, straight, uniform fiber.

The equation governing the spatial and temporal distribution of the subthreshold transmembrane potential, V_m, when an electric field is applied is

$$V_m + \tau \frac{\partial V_m}{\partial t} - \lambda^2 \frac{\partial^2 V_m}{\partial x^2} = -\lambda^2 \frac{\partial E_x}{\partial x} \tag{1}$$

where τ is the membrane time constant, λ is the fiber length constant, and E_x is the component of the electric field that is parallel to the fiber axis (x). The left-hand side of Equation 1 is the conventional one-dimensional (1-D) cable equation (e.g. see 6) with a source term on the right-hand side called the activating function. Here, it is written as $-\lambda^2 \partial E_x/\partial x$ (7), but, in the absence of any time-varying magnetic fields, it can be expressed as $\lambda^2 \partial^2 V_e/\partial x^2$, where V_e is the extracellular potential (8, 34).

For steady-state stimulation with an extracellular potential that varies little over distances on the order of a length constant, the second and third terms on the left-hand side of Equation 1 are negligible; the transmembrane potential is thus equal to the activating function. For short pulses or when the scale of the variation of the extracellular potential distribution is comparable to or smaller than the length constant, the resultant transmembrane potential distribution can be quite different from the activating function. Then, the full cable equation (Equation 1) determines V_m (9, 10).

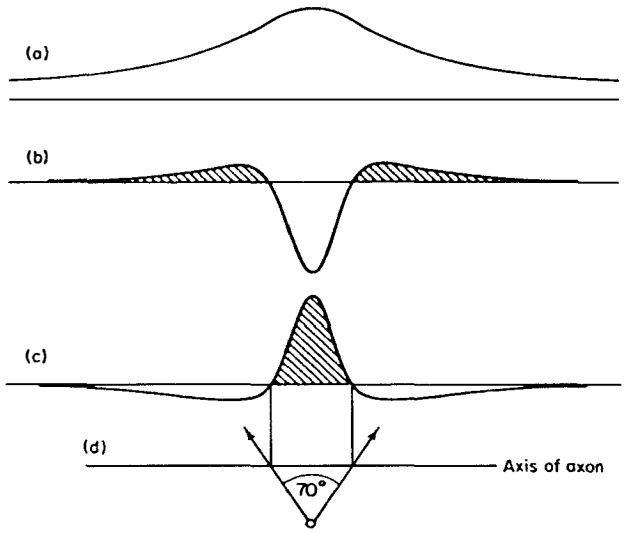

Figure 1 The activating function during electrical stimulation. (*a*) Calculated extracellular potential along a fiber produced by a unipolar spherical electrode, and the activating functions for (*b*) anodal and (*c*) cathodal stimulation. *Shaded areas*, Regions where depolarization is expected. (*d*) The position of the electrode compared with the fiber. (Reproduced from reference 11, with permission from Academic Press, Ltd.)

Figure 1 shows the extracellular potential and the activating function along a fiber produced by a steady-state current applied through a point extracellular electrode (11). If the electrode is a cathode (Figure 1*c*), then near to it the fiber is strongly depolarized (*shaded*), but, farther away from the cathode, we observe two hyperpolarized regions, called virtual anodes. Depolarization produces excitation, so excitation occurs directly under the cathode (called cathode-make excitation). If the electrode is an anode (see Figure 1*b*), then near it the fiber is hyperpolarized, but we observe two depolarized (*shaded*) areas, called virtual cathodes. Anodal excitation occurs at the virtual cathodes (called anode-make excitation). During cathodal stimulation, excitation occurs near the cathode at a relatively low stimulus strength; during anodal stimulation, excitation occurs at the virtual cathode with a relatively high stimulus strength. These findings are easily explained by computing the distribution of the activating function (11). The ratio of the maximum values of the activating function for cathodal and anodal stimulation is ~5 to 1. If the electrode is placed more than a few length constants from the fiber, the ratio of cathodal and anodal threshold stimulus strengths is also ~5 to 1 (12).

Virtual anodes can arise during cathodal stimulation and can affect the dynamics of the action potential. For instance, an action potential cannot propagate through a region that is hyperpolarized by >50 mV below resting potential (13). If the stimulus is strong enough, an action potential that is excited near a cathode will be blocked by the virtual anode. This effect has been observed experimentally by

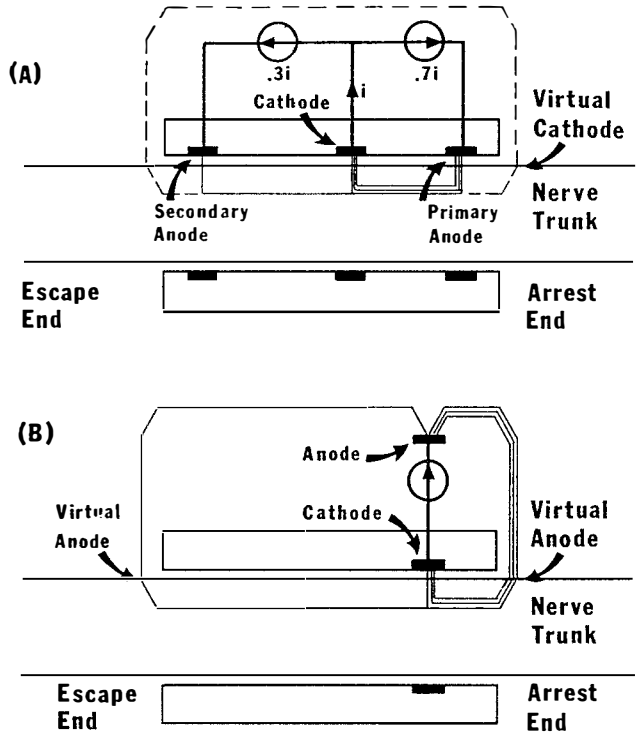

Figure 2 Unidirectional "block" of action potential propagation. (*A*) A tripolar cuff electrode as described by van den Honert & Mortimer (17). (*B*) A simplified design that uses a single cathode in the cuff and allows the anodes to be "virtual." If the stimulus current is chosen properly, an action potential excited at the cathode will be blocked by the strong virtual anode (arrest end), but will propagate through the weak virtual anode (escape end). (Reproduced from reference 14, with permission of Blackwell Scientific Publications, Inc.)

Ranck (12), and has been exploited by Ungar et al (14), who modified the activating function by surrounding the cathode with an insulating cuff (Figure 2). Because Ungar et al do not center the cathode within the cuff (Figure 2*B*), the virtual anode on one side of the cuff is stronger than the virtual anode on the other side. A range of stimulus strengths can be found for which action potentials are blocked at the stronger virtual anode but not at the weaker one. This asymmetrical block generates an action potential that propagates in only one direction. The development of such undirectional block techniques has been useful in functional electrical stimulation (15–19).

The presence of a virtual anode can also reverse the recruitment order for motor axons. Axons within a nerve bundle have a variety of diameters. The factor of λ^2 in the activating function implies that large-diameter fibers are excited more easily than are small-diameter fibers (6). However, the small-diameter fibers control

finer motor movements (6); therefore, their selective stimulation would provide better control over muscle force. Blocks that occur at the virtual anode allow such physiological recruitment. If the stimulus is strong enough, all fibers—large and small—are excited at the cathode, but propagation along the large fibers is more easily blocked by the virtual anode. Therefore, action potentials propagate far from the electrode only in the small fibers (13, 18–20). Another way to affect recruitment order is to use different current waveforms to inactivate strongly stimulated fibers selectively (21). In this scheme, a prepulse is applied to depolarize the axons slowly. This subthreshold depolarization inactivates the sodium channel ($h = 0$), so that the subsequent stimulus pulse will find the fiber in a refractory state. The larger the fiber, the more inactivated its sodium channels become, so the second stimulus pulse will tend to excite more of the smaller-diameter fibers.

The activating function also describes magnetic stimulation of peripheral-nerve fibers (7, 22–24). The activating function produced during magnetic stimulation by a circular coil is shown in Figure 3. Typically, the coil is held so that the fiber (*dashed line*) lies below one edge of the coil (*bold circle*). The fiber is depolarized at a virtual cathode (*minus symbol*) and is hyperpolarized at a virtual anode (*plus*

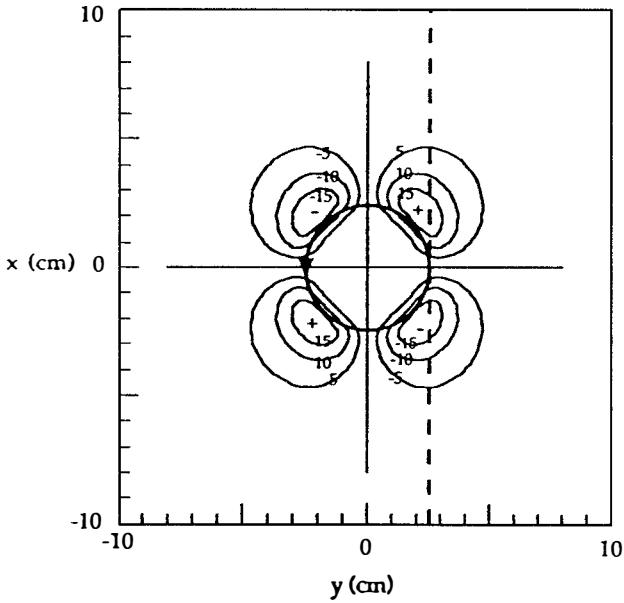

Figure 3 The activating function during magnetic stimulation. A contour plot of the calculated spatial derivative of the electric field in the x-direction, $\partial E_x/\partial x$, is displayed as a function of position with contour lines given in increments of 5 mV/cm^2. *Bold circle*, position and geometry of the coil; *dashed line*, position of a nerve. −, Location at which the nerve is maximally depolarized; +, position of maximum hyperpolarization. [Reproduced from reference 7 with permission (copyright 1990, IEEE)].

symbol), which are separated in Figure 3 by ~40 mm. The distance between the virtual anode and the virtual cathode depends on the distance of the nerve to the coil; if the nerve is a small fraction of a coil radius below the coil, the spatial distribution of the activating function becomes more complex (25). The virtual anode and cathode switch places when the polarity of the coil current is reversed, which is predicted to result in a latency shift of the action potential when measured far from the stimulus site (7). Maccabee et al (26) observed such a latency shift during in vitro magnetic stimulation of a pig phrenic nerve (Figure 4*a*). Using a "figure eight" coil, they measured the electric field, activating function, and response latency for both coil current polarities. They reported a 36-mm separation between the virtual anode and cathode as calculated from the spatial derivative of the measured induced electric field. Then they found a response latency shift of 1.2 ms in the nerve, which corresponds to a separation between the virtual anode and cathode of 34.7 mm, when using their independent measurement of nerve conduction velocity, 28.9 m/s. Nilsson et al (27) reported similar findings during in vivo stimulation of human median nerve. An activating function like the one produced by a single electrode (Figure 1) can be induced during magnetic stimulation by a four-leaf coil (28–30). Depolarization, leading to excitation of peripheral nerves in vitro, occurs directly under the center of the four-leaf coil for one coil-current polarity, but hyperpolarization results for the opposite polarity.

We have been treating nerve axons as if they were uniform fibers, which is a reasonable approximation for unmyelinated axons. A myelinated axon, however, is surrounded by a nearly insulating myelin sheath except at discrete excitable patches of membrane—the nodes of Ranvier. Myelinated axons can be represented by a composite cable equation (31, 32), in which the nodes and myelinated portions of the nerve each satisfy Equation 1, but have different space and time constants. When the applied electric field is not spatially localized, the composite model can be averaged over the fiber length (31, 32). Homogenization produces an equivalent cable equation of the form in Equation 1 (31). During conventional magnetic stimulation, the induced electric fields are so diffuse that this homogenized cable model almost always applies. However, during electric stimulation, if an electrode is placed close to an axon (at a distance comparable with or smaller than the node separation, which is on the order of a millimeter), the full composite model is required. The composite cable model has been solved by using the method of lines (23). A finite difference method (33) that is based on an earlier discrete model of nerve conduction by McNeal (34) can also be used.

The electric field along the fiber must be nonuniform for the activating function to be nonzero. This nonuniformity can arise in several ways. For example, the applied electric field may be uniform, but there might be an inhomogeneity in the conductivity of the extracellular volume conductor (e.g. see 35). Maccabee et al (26, 36) have performed experiments to evaluate the effect of such inhomogeneities on excitation (Figure 4*b*). Using magnetic stimulation of a sheep phrenic nerve, they found that, by placing two Lucite cylinders in the saline bath adjacent to the nerve, they changed both the response latency and the site of action-potential

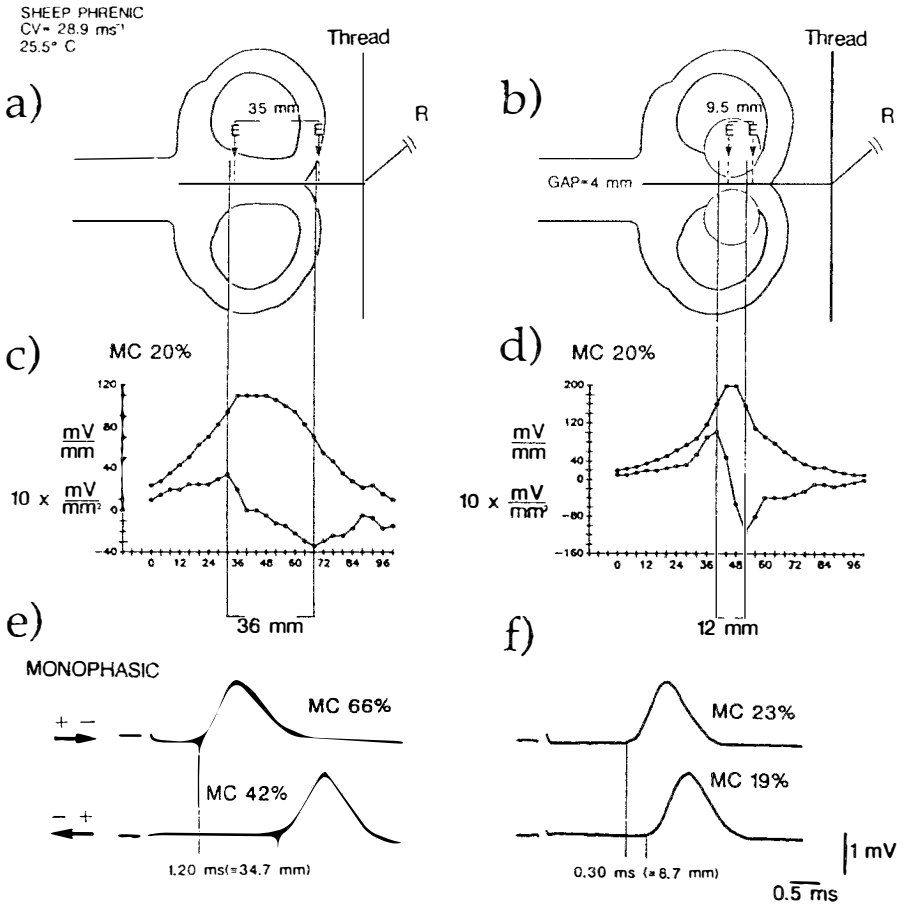

Figure 4 In vitro magnetic stimulation of sheep phrenic nerve. (*a*) The position of the figure-eight coil relative to the nerve. The thread indicates where the nerve is raised from the saline for extracellular potential recording at the site marked "R." (*b*) To evaluate the effect of an inhomogeneous volume conductor, a similar experiment was performed, but with two Lucite cylinders surrounding the nerve. (*c* and *d*) The measured electric field and its spatial derivative along the direction parallel to the nerve. (*e* and *f*) The action potential, recorded extracellularly, caused by magnetic stimulation with both polarities of the coil current. The strength of the magnetic-coil (MC) stimulation is given as a percentage of the maximum output of the stimulator. (Reproduced from reference 26, with permission of Cambridge University Press.)

excitation significantly. Inhomogeneities may cause excitation at local "hot spots," where the electric field is focused, such as at small openings (foramina) in a bone. Maccabee et al (37) suggest that such hot spots may cause excitation of nerve roots near the point where they emerge from the intervertebral foramina.

The results discussed above apply to long, straight, uniform fibers. Other mechanisms of stimulation arise if a fiber is terminated, nonuniform, or curved. We first consider how an electric field stimulates a nerve fiber at its terminus (33, 38–40). At the terminus, the intracellular axial current is zero, so all of the current must be flowing radially. There, a smaller electric field may be required to drive current across the membrane, than is required to stimulate the long axon body by the electric field gradient mechanism. Stimulation at the fiber terminus may have the lowest stimulus threshold in many instances (41–43). For a fiber that is more than several length constants long, significant polarization occurs only near the ends of the fiber (depolarization at one end and hyperpolarization at the other).

Nonuniform fiber properties can also lead to nerve depolarization. Consider a long, straight fiber that is oriented parallel to a uniform electric field. If its radius experiences a step change, current will be forced to flow across the membrane. If the fiber diameter gets larger, then current flows in, and V_m is negative (hyperpolarization); if the fiber diameter gets smaller, the current flows out, and V_m is positive (depolarization) (5). Similar results are obtained if the extracellular or intracellular resistivity changes instead of the fiber diameter.

Changes or variations in fiber trajectory can also cause nerve polarization (23, 26, 36, 44, 45). If a fiber is abruptly bent, the bend acts as a focal point for excitation. If a fiber is bent toward the electric field, it is hyperpolarized; if the fiber is bent away from the electric field, it is depolarized (44). A general way to treat this effect is to include the local fiber tract trajectory and the local electric field along the fiber in the activating function, as in 23. Specifically, one should calculate the component of the electric field or of the electric field gradient that is in the direction parallel to the local fiber tract direction. Because nerves follow sinuous paths through the body, changes in fiber trajectory may play an important role in electrical stimulation. For instance, this effect may provide another explanation for the stimulation of nerve roots at the intervertebral foramina.

EXCITATION OF CORTICAL TISSUE

Some motor neurons in the cerebral cortex are oriented perpendicularly to the cortical surface. The dendritic tree at the distal end of these neurons coalesces into the soma or cell body. At the proximal end is the axon. If an applied electric field is directed from the cortical surface inward, the dendrites are hyperpolarized, and the axon is depolarized. This mode of stimulation should be excitatory. If the stimulus is strong enough, the axon will be depolarized to threshold, eliciting an action potential. On the other hand, if the applied electric field is directed outward from the cortical surface, the dendrites are depolarized, and the axon is

hyperpolarized, resulting in no excitation. If the applied electric field is directed parallel to the cortical surface, there should be little or no effect on these neurons [except, perhaps, where the axon changes direction and enters the white matter (44)]. Because of the many cortical folds (i.e. gyri and sulci), the cortical surface is seldom oriented parallel to the surface of the skull. This complicates our analysis of brain stimulation, because predicting the degree to which a neuron is stimulated by an electric field also requires knowing that neuron's orientation.

Several groups (see 44, 46–48) have analyzed the problem of central nervous excitation quantitatively, using models of the detailed structure of a single cortical neuron. In general, the site of stimulation is in the axon (47,48). Moreover, the time course of the transmembrane potential plays an important role in determining the site of excitation (48).

Transcranial excitation of the brain is one of the most important applications of magnetic stimulation. Although electrodes attached to the scalp can be used to activate neurons in the brain, the high resistance of the skull shunts most of the current through the scalp, making electric brain stimulation quite painful and relatively ineffective. Transcranial magnetic stimulation, on the other hand, is minimally affected by the skull and is virtually painless.

Besides the different degree of pain involved, there are other important differences between transcranial electric and magnetic stimulation of the brain. First, during magnetic stimulation, the direction of the electric field is approximately tangential, that is, parallel to the inside surface of the skull. During electric stimulation, however, the electric field has both radial and tangential components, and it is entirely radial directly below the anode (recall that an outward current across the cortex is believed to cause stimulation), where stimulation is thought to occur. Therefore, transcranial electric stimulation may preferentially excite neurons at gyri near the inside surface of the skull, whereas transcranial magnetic stimulation may preferentially excite neurons within sulci. There are also latency differences in surface-recorded electromyographic responses in electrical and magnetic stimulation (49, 50). The response latency in the contracting muscle during magnetic stimulation was found to be ~2 ms longer than it was during electric stimulation. These researchers explained their results by suggesting that magnetic stimulation activates corticospinal neurons trans-synaptically, whereas electric stimulation activates corticospinal neurons directly (for alternative points of view, see 45, 51). Whether the difference in electric field orientation and the difference in response latency are related is unknown.

EXCITATION OF CARDIAC TISSUE

Cardiac muscle is fundamentally different from nerve tissue because the heart is a syncytium. The intracellular space of each cardiac cell is coupled to its neighbor's through intercellular channels. Thus, current can flow from the interior of one cell to the interior of another without crossing a cell membrane. To a first approximation,

therefore, cardiac tissue acts like a three-dimensional (3-D) cable. The bidomain model (for a general discussion, see 52) is a mathematical model of this 3-D cable. The model is based on Ohm's law and the continuity of current. The intracellular and interstitial spaces can be assigned different conductivities. Any current leaving the intracellular space and entering the interstitial space must pass across the cell membrane, either through the membrane capacitance or else through the membrane conductance (which may be nonlinear and voltage and time-dependent). The bidomain model is a continuum model, in that it does not take into account the discrete cellular structure of the tissue.

One important feature of the bidomain model is that it can take into account the electrical anisotropy of the tissue, that is, the tendency for the electrical conductivity to be different when measured along different directions. More specifically, the electrical conductivity within the intracellular and interstitial spaces is anisotropic (and can be described by individual conductivity tensors); however, the degree of anisotropy is not necessarily the same in both compartments. The ratio of conductivities parallel to and perpendicular to the fibers in the intracellular space is $\sim$10:1, whereas this ratio in the extracellular space is $\sim$2.5:1 (53). These unequal anisotropy ratios may be responsible for many of the interesting electrical features and phenomena exhibited by cardiac tissue.

If a unipolar, extracellular cathode excites a two-dimensional (2-D) sheet of passive cardiac tissue (i.e. a bidomain with unequal anisotropy ratios), the transmembrane potential will exhibit adjacent regions of depolarization and hyperpolarization (54). The tissue is strongly depolarized directly below the cathode but weakly hyperpolarized a few millimeters from it in the direction parallel to the myocardial fibers (Figure 5). Although this phenomenon surprised the cardiology community, the reason for this behavior is clear when one understands the analogy between cardiac tissue and peripheral nerves. Hyperpolarized cardiac tissue (i.e. the virtual anode) is analogous to the virtual anode produced during extracellular stimulation of a peripheral nerve (Figure 1). Such virtual electrode effects in cardiac tissue have been predicted theoretically (55) and were later observed experimentally (56–58). If the polarity of the stimulating current is changed so that the stimulation arises from an anode rather than from a cathode, then the tissue will be hyperpolarized under the anode and depolarized at a nearby virtual cathode. Depolarization at the virtual cathode provides a mechanism for anode-make excitation in cardiac tissue (58, 59), just as it did for peripheral nerves.

Besides cathode- and anode-make excitation, cardiac tissue also exhibits cathode-break and anode-break excitation. Dekker (60) measured the thresholds for four mechanisms of excitation in resting cardiac tissue during extracellular stimulation. He found that the order (from the lowest stimulus threshold value to the highest) is (*a*) cathode make, (*b*) anode make, (*c*) cathode break, and (*d*) anode break. Break excitation in cardiac tissue may be fundamentally different than in a nerve (58, 59). Anode-break excitation follows the turning off of the anodal stimulus. In the Hodgkin-Huxley explanation of anode break (61), the anodal pulse removes sodium inactivation ($h = 1$). This mechanism does not appear to apply

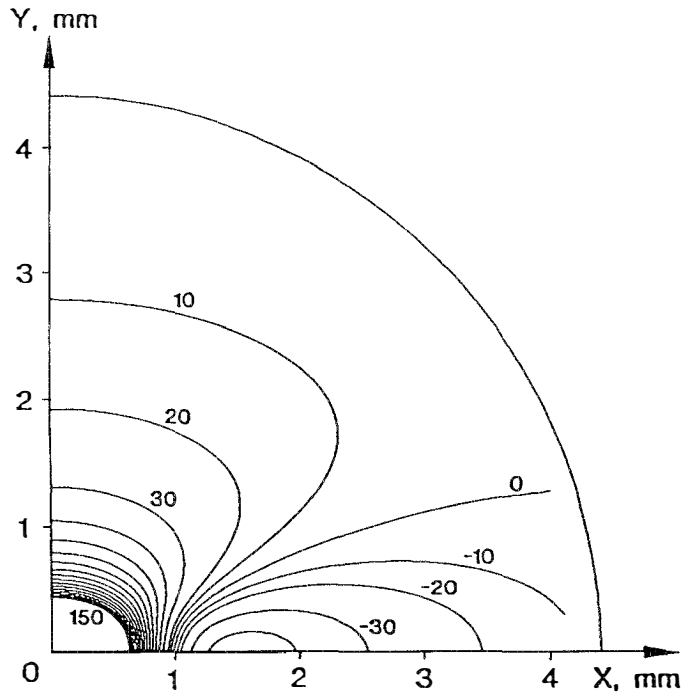

Figure 5 The calculated steady-state transmembrane potential, V_m, produced by an extracellular point source in a passive, 2-D bidomain. The cathode is located at the origin. Only one quadrant of the x-y plane is shown. In the other three quadrants V_m is found by reflecting the curves across the x- and y-axes. The myocardial fibers are oriented parallel to the x-axis, and nominal conductivity values are used (unequal anisotropy ratios). Contour lines are drawn every 10 mV (source strength = 4 mA/mm). The contour lines near the source are very close together and are not drawn. (Reproduced from reference 54, with permission of the Biophysical Society.)

to the heart, because the slow sodium inactivation gate is already completely open ($h = 1$) in resting cardiac tissue (62).

Break stimulation in cardiac tissue may arise from an interaction of virtual anodes and cathodes at the end of a stimulus pulse (58, 59). During a cathodal stimulus, an area of strong depolarization exists under the cathode, and regions of hyperpolarization exist at the virtual anodes. When the stimulus is turned off, the strong depolarization under the cathode decays and diffuses into the region that contained the virtual anode. The sodium channels in this anodic region are not inactivated, so the tissue there is excitable (the tissue under the cathode would have its sodium channel completely inactivated by the strong depolarization and would therefore be unexcitable). If diffusion of transmembrane potential is strong enough, an action potential can arise in this excitable region. The resulting wave front cannot propagate toward the cathode but could propagate outward away from

the cathode in the direction parallel to the fibers. Anode-break excitation arises by a similar mechanism to that of cathode-break excitation. Depolarization at the virtual cathodes diffuses into the excitable tissue under the anode, triggering a wave front that can propagate perpendicularly to the fiber direction (58, 59). Ranjan et al (63) recently proposed a different mechanism for anode break excitation in cardiac tissue, based solely on membrane channel kinetics. The relative importance of these two mechanisms for anode break excitation has yet to be resolved.

One important difference between cardiac muscle and nerve tissue is that, in the heart, an action potential can propagate both parallel and perpendicularly to the fiber axis. A nerve action potential, having been excited by cathodal stimulus, might be blocked by a virtual anode. However, in cardiac tissue the analogous block would occur only in the direction parallel to the fibers. Thus, propagation perpendicular to the fibers could still occur. Action-potential wave fronts cannot pass through a virtual anode, but they can circle around it. The concept of anode block in nerves translates into the more subtle notions of unidirectional block and reentry in cardiac tissue. Thus, cardiac tissue gives rise to a wider variety of behaviors after electrical stimulation than does a peripheral nerve.

Under certain circumstances, the virtual anode does not hinder propagation originating at the cathode, but instead may help it. When one stimulus excites the heart, and then a strong second stimulus is applied at the same position during the repolarization phase of the first action potential, the action potential evoked by the second stimulus may not be able to propagate because the surrounding tissue is refractory. However, hyperpolarization shortens the duration of the refractory period (a process called "de-excitation"). If the second stimulus is timed correctly, the virtual anode created by the second stimulus may shorten the refractory period of the first wave front locally. This occurs while the surrounding tissue remains refractory and unexcitable, thus creating an excitable path along the direction parallel to the fibers. Such behavior may influence the strength-interval curves for cardiac tissue (64) and may lead to "quatrefoil"reentry (65, 66; Figure 6). Such effects may play an important role during defibrillation (67, 68).

So far, we have considered unipolar stimulation of cardiac tissue with the stimulus applied through a single small electrode. During cardiac defibrillation, strong electric shocks are applied over large regions of the heart. One of the central unanswered questions about defibrillation is, What are the mechanisms by which a nearly uniform electric field affects cardiac tissue (69)?

Frazier et al (70) suggest that the extracellular potential gradient determines the transmembrane potential experienced by the tissue. The mechanism underlying Frazier et al's hypothesis is that the discrete cellular structure of cardiac tissue causes each cell to be depolarized at one end and hyperpolarized at the other (Figure 7). This hypothesis is predicated on the assumption that the resistance of the intercellular junctions between cells is large compared with the resistance of the myoplasm within cells. Several theoretical studies have shown that a large junctional resistance can lead to a sawtooth pattern of transmembrane potential when a 1-D chain of cells is placed in a uniform electric field (71–74). Half of each

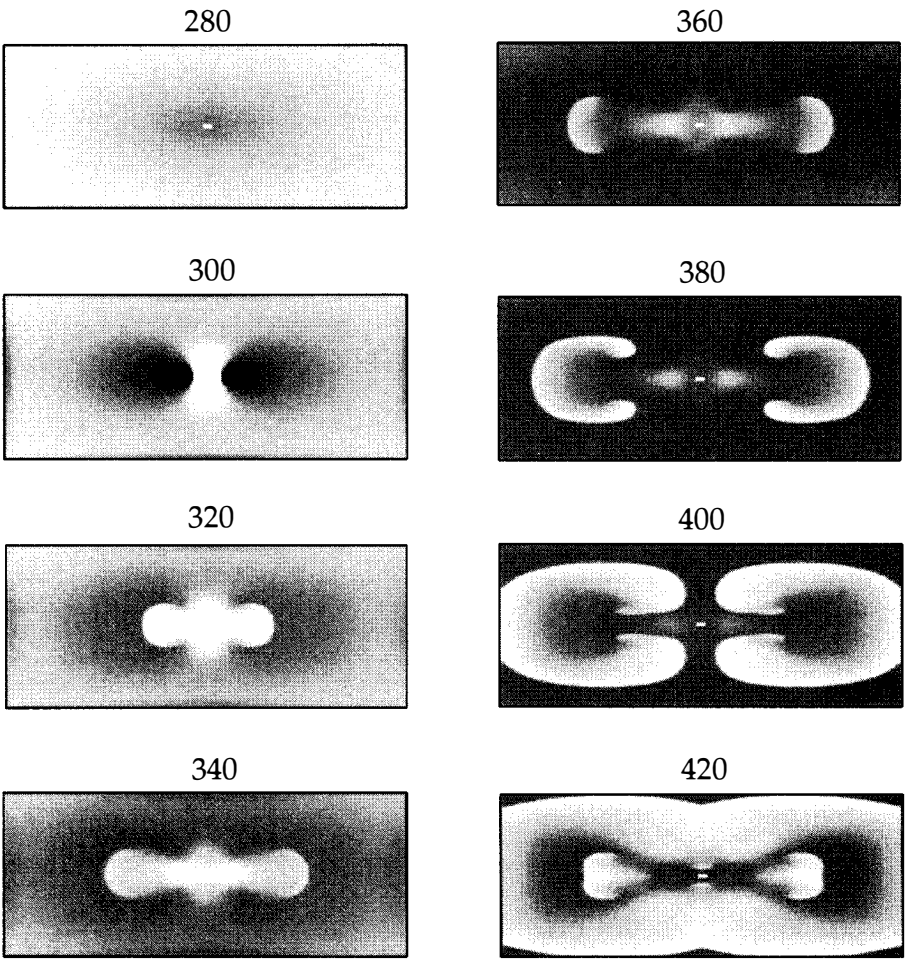

Figure 6 Wavefront dynamics after a cathodal, 20-ms premature pulse; S1-S2 interval = 280 ms; S2 strength = 20 mA. Fibers are horizontal, and the electrode is located in the center of each panel. *Gray* represents resting, *white* is depolarized, and *black* is hyperpolarized. The number above each panel is time in milliseconds. (Adapted from reference 65.)

cell is depolarized, and half is hyperpolarized. The degree of the membrane polarization is predicted to be nearly proportional to the magnitude of the extracellular electric field, and this prediction is consistent with the observations of Frazier et al. However, the sawtooth effect has never been observed experimentally (75–77).

Trayanova et al (78) suggested an alternative to the sawtooth mechanism for exciting cardiac tissue with an electric field. Just as a curved nerve fiber may be polarized by a uniform electric field (e.g. see 23), so may a curved fiber in cardiac tissue. Trayanova et al calculated the transmembrane potential induced

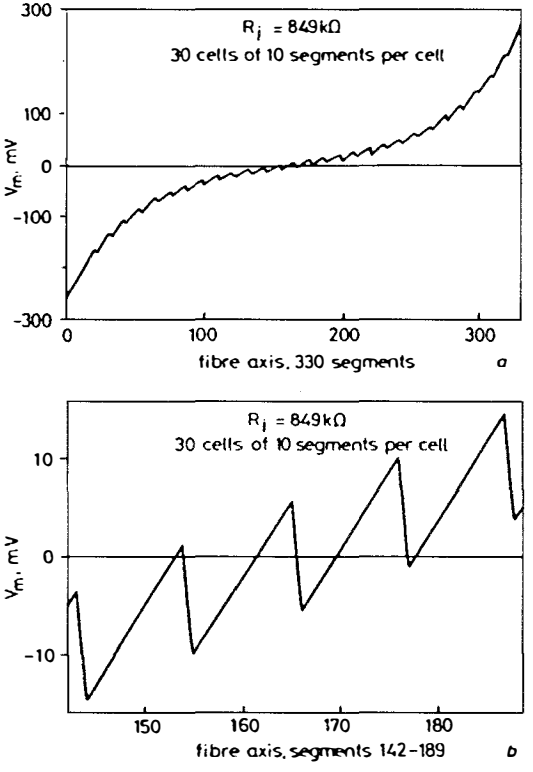

Figure 7 Sawtooth pattern of transmembrane potential along a 1-D strand of cardiac tissue in a uniform electric field. The strand is 30 cells long; the junctional resistance between cells is 849 kOhm. (*a*) The calculated transmembrane potential along the entire length of the fiber; (*b*) the central portion of the fiber on an expanded scale. (Reproduced from reference 72, with permission of The Institution of Electrical Engineers.)

throughout a spherical bidomain with curving fiber tracts when it is placed in a uniform electric field. They found that polarization is large at the surface of the sphere and that a smaller (but non-negligible) polarization occurs throughout the tissue bulk. The surface polarization arises because of current redistribution between the intracellular and extracellular spaces at the tissue-bath interface. The tissue is strongly polarized at the tissue surface—an effect much like that of the terminated nerve fiber. The polarization in the tissue bulk, on the other hand,

Figure 8 The effect of a uniform S2 stimulus on the transmembrane voltage (V_m). (*A*) Measurements from a rabbit heart (percentage of action-potential amplitude); (*B*) bidomain model results. The S2 electrode near the base of the heart or the top of the model was cathodal. The S2 strength was 312 mA. (Reproduced from reference 82, with permission of the Biophysical Society.)

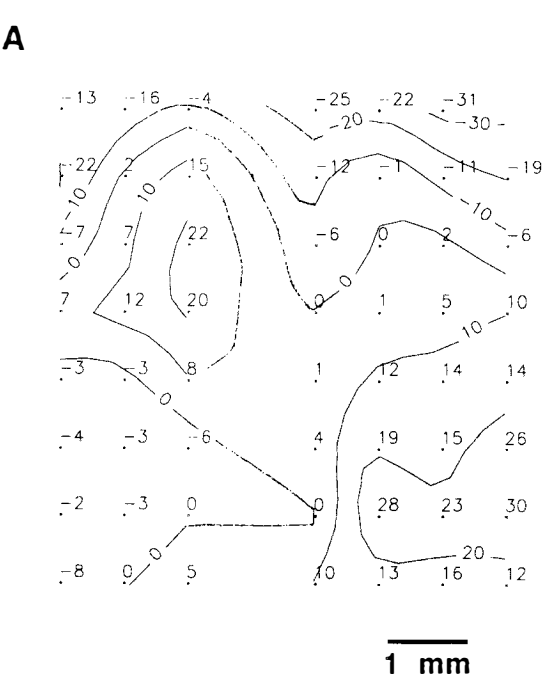
Uniform
A
1 mm
B
ΔV_m (mV); US2
2 mm
-20
0
20

arises from unequal anisotropy ratios and curved fiber geometry, an effect much like that of the curved nerve fiber (78, 79). For tissue located more than a few length constants from the sphere surface, the bulk term is the dominant contribution to the transmembrane potential. This bulk polarization provides an alternative to the sawtooth mechanism for explaining the effect of strong electrical stimuli on cardiac tissue.

Tissue inhomogeneities provide another mechanism for electrical excitation of cardiac tissue (69, 69a). This mechanism resembles the sawtooth mechanism described earlier, except that it is exhibited at a larger length scale. The discrete resistances represent coupling between relatively isolated patches of tissue, with each patch containing many cells. Such structures might exist in diseased tissue.

At present, we do not know which of these mechanisms is primarily responsible for defibrillation. Sobie et al (80) have presented a generalized activating function, which is an extension of the 1-D activating function in Equation 1, to predict virtual electrode patterns. Experimental results (Figure 8) by Entcheva et al (81) and Knisley et al (82) suggest that the bidomain model predicts many of the important features of electrical stimulation of cardiac tissue, even for cases in which the electrode geometry is much more complex than a simple unipolar electrode.

CONCLUDING REMARKS

The bidomain model provides a unified framework to treat electrical stimulation of peripheral nerves, cortical neurons, and cardiac tissue. We see that the 1-D cable model of a single myelinated or unmyelinated axon can be described by a 1-D bidomain model. A bundle of axons (such as a fascicle) can be modeled as a 2-D bidomain. Cardiac muscle syncytium can be described by a 3-D bidomain model, in which the extracellular and intracellular spaces are now characterized by conductivity tensors that are assumed to have the same principal directions, but different principal conductivities. Finally, cortical neural tissue appears to be the most complex, consisting of a composite of 1-, 2-, and 3-D bidomains.

Bidomain models can be used to reveal quantitative and qualitative features about electrically excitable tissue, as well as to predict many aspects of their behavior. They are extremely useful in describing the response of different types of excitable tissues to electric fields that arise from charge redistribution (electrical stimulation) and/or from time-varying magnetic fields (magnetic stimulation) in a self-consistent manner. They also have proved useful for predicting tissue behavior, for testing hypotheses about possible excitation mechanisms, for designing novel electrophysiological experiments, and for interpreting their findings. Whereas the bidomain model rationally applies Maxwell's equations to tissues with multiple compartments, it is nonetheless a phenomenological model, in that it does not explicitly elucidate the fundamental physical basis for tissue excitability.

ACKNOWLEDGMENTS

BJR was supported in part by the National Institutes of Health grant R01-HL57207. We also thank Carlo Pierpaoli for making many helpful suggestions about this chapter.

LITERATURE CITED

1. Durand DM. 1995. Electrical stimulation of excitable tissue. In *The Biomedical Engineering Handbook*, ed. JD Bronzino, pp. 229–51. Boca Raton, FL: CRC Press
2. Coburn B. 1989. Neural modeling in electrical stimulation. *Crit. Rev. Biomed. Eng.* 17:133–78
3. Rattay F. 1990. *Electrical Nerve Stimulation: Theory, Experiments, and Applications*. New York: Springer-Verlag. 264 pp.
4. Reilly JP. 1992. *Electrical Stimulation and Electropathology*. Cambridge, UK: Cambridge Univ. Press. 563 pp.
5. Roth BJ. 1994. Mechanisms for electrical stimulation of excitable tissue. *Crit. Rev. Biomed. Eng.* 22:253–305
6. Plonsey R, Barr RC. 1988. *Bioelectricity, A Quantitative Approach*. New York: Plenum. 305 pp.
7. Roth BJ, Basser PJ. 1990. A model of the stimulation of a nerve fiber by electromagnetic induction. *IEEE. Trans. Biomed. Eng.* 37:588–97. Erratum. 1992. *IEEE Trans. Biomed. Eng.* 39:1211
8. Rattay F. 1986. Analysis of models for external stimulation of axons. *IEEE Trans. Biomed. Eng.* 33:974–77
9. Plonsey R, Barr RC. 1995. Electric field stimulation of excitable tissue. *IEEE Trans. Biomed. Eng.* 42:329–36
10. Warman EN, Grill WM, Durand D. 1992. Modeling the effects of electric fields on nerve fibers: determination of excitation thresholds. *IEEE Trans. Biomed. Eng.* 39:1244–54
11. Rattay F. 1987. Ways to approximate current-distance relations for electrically stimulated fibers. *J. Theor. Biol.* 125:339-49
12. Ranck JB Jr. 1975. Which elements are excited in electrical stimulation of mammalian central nervous system: a review. *Brain Res.* 98:417–40
13. Fang Z-P, Mortimer JT. 1991. Selective activation of small motor axons by quasitrapezoidal current pulses. *IEEE Trans. Biomed. Eng.* 38:168–74
14. Ungar IJ, Mortimer JT, Sweeney JD. 1986. Generation of unidirectionally propagating action potentials using a monopolar electrode cuff. *Ann. Biomed. Eng.* 14:437-50
15. Sweeney JD, Mortimer JT, Bodner DR. 1989. Acute animal studies on electrically induced collision block of pudendal nerve motor activity. *Neurol. Urodyn.* 8:521-36
16. van den Honert C, Mortimer JT. 1981. A technique for collision block of peripheral nerve: single stimulus analysis. *IEEE Trans. Biomed. Eng.* 28:373–78
17. vanden Honert C, Mortimer JT. 1979. Generation of unidirectionally propagated action potentials in a peripheral nerve by brief stimuli. *Science* 206:1311–12
18. Fang Z-P, Mortimer JT. 1991. Alternate excitation of large and small axons with different stimulation waveforms: an application to muscle activation. *Med. Biol. Eng. Comput.* 29:543–47
19. Fang Z-P, Mortimer JT. 1991. A method to effect physiological recruitment order in electrically activated muscle. *IEEE Trans. Biomed. Eng.* 38:175–79

20. Tai CF, Jiang DZ. 1994. Selective stimulation of smaller fibers in a compound nerve trunk with single cathode by rectangular current pulses. *IEEE Trans. Biomed. Eng.* 41:286–91
21. Grill WM, Mortimer JT. 1997. Inversion of the current-distance relationship by transient depolarization. *IEEE Trans. Biomed. Eng.* 44:1–9
22. Durand D, Ferguson AS, Dalbasti T. 1989. Induced electric fields by magnetic stimulation in non-homogeneous conducting media. *Proc. Ann. Int. Conf. IEEE-EMBS* 11:1252–53
23. Basser PJ, Roth BJ. 1991. Stimulation of a myelinated nerve axon by electromagnetic induction. *Med. Biol. Eng. Comput.* 29:261–68
24. Basser PJ, Wijesinghe RS, Roth BJ. 1992. The activating function for magnetic stimulation derived from a three-dimensional volume conductor model. *IEEE Trans. Biomed. Eng.* 39:1207–10
25. Basser PJ. 1994. Focal magnetic stimulation of an axon. *IEEE Trans. Biomed. Eng.* 41:601–6
26. Maccabee PJ, Amassian VE, Eberle LP, Cracco RQ. 1993. Magnetic coil stimulation of straight and bent amphibian and mammalian peripheral nerve in vitro: locus of excitation. *J. Physiol.* 460:201–19
27. Nilsson J, Panizza M, Roth B J, Basser PJ, Cohen LG, et al. 1992. Determining the site of stimulation during magnetic stimulation of a peripheral nerve. *Electroencephalogr. Clin. Neurophysiol.* 85:253–64
28. Roth B J, Turner R, Cohen LG, Hallett M. 1990. New coil design for magnetic stimulation with improved focality. *Mov. Disord.* 5(Suppl. 1):32
29. Roth B J, Maccabee PJ, Eberle LP, Amassian VE, Hallett M, et al. 1994. In-vitro evaluation of a four-leaf coil design for magnetic stimulation of peripheral nerve. *Electroencephalogr. Clin. Neurophysiol.* 93:68–74
30. Esselle KP, Stuchly MA. 1992. Neural stimulation with magnetic fields: analysis of induced electric fields. *IEEE Trans. Biomed. Eng.* 39:693–700
31. Basser PJ. 1993. A cable equation for a myelinated axon derived from its microstructure. *Med. Biol. Eng. Comput.* 31: S87–92
32. Andrietti F, Bernardini G. 1984. Segmented and "equivalent" representation of the cable equation. *Biophys. J.* 46:615–23
33. Nagarajan SS, Durand DM. 1996. A generalized cable equation for magnetic stimulation of axons. *IEEE Trans. Biomed. Eng.* 43:304–12
34. McNeal DR. 1976. Analysis of a model for excitation of a myelinated nerve. *IEEE Trans. Biomed. Eng.* 23:329–37
35. Kobayashi M, Ueno S, Kurokawa T. 1997. Importance of soft tissue inhomogeneity in magnetic peripheral nerve stimulation. *Electroencephalogr. Clin. Neurophysiol.* 105:406–13
36. Maccabee PJ, Nagarajan SS, Amassian VE, Durand DM, Szabo AZ, et al. 1998. Influence of pulse sequence, polarity and amplitude on magnetic stimulation of human and porcine peripheral nerve. *J. Physiol.* 513:571–85
37. Maccabee PJ, Amassian VE, Eberle LP, Rudell AP, Cracco RQ, et al. 1991. Measurement of the electric field induced into inhomogeneous volume conductors by magnetic coils: application to human spinal neurogeometry. *Electroencephalogr. Clin. Neurophysiol.* 81:224–37
38. Altman KW, Plonsey R. 1990. Analysis of excitable cell activation: relative effects of external electrical stimuli. *Med. Biol. Eng. Comput.* 28:574–80
39. Rubenstein JT. 1993. Axon termination conditions for electrical stimulation. *IEEE Trans. Biomed. Eng.* 40:654–63
40. Nagarajan SS, Durand DM, Warman EN 1993. Effects of induced electric fields on finite neuronal structures: a simulation

study. *IEEE Trans. Biomed. Eng.* 40:1175-88

41. Nagarajan SS, Durand DM. 1992. Determination of excitation sites during magnetic stimulation of nerve fibers. *Proc. Ann. Int. Conf. IEEE-EMBS* 14:1426–27
42. Reilly JP, Freeman VT, Larkin WD. 1985. Sensory effects of transient electrical stimulation: evaluation with a neuroelectric model. *IEEE Trans. Biomed. Eng.* 32: 1001–11
43. Reilly JP. 1989. Peripheral nerve stimulation by induced electric currents: exposure to time-varying magnetic fields. *Med. Biol. Eng. Comput.* 27:101–10
44. Tranchina D, Nicholson C. 1986. A model for the polarization of neurons by extrinsically applied electric fields. *Biophys. J.* 50:1139–56
45. Amassian VE, Eberle L, Maccabee PJ, Cracco RQ. 1992. Modelling magnetic coil excitation of human cerebral cortex with a peripheral nerve immersed in a brain-shaped volume conductor: the significance of fiber bending in excitation. *Electroencephalogr. Clin. Neurophysiol.* 85:291-301
46. Hause L. 1975. A mathematical model for transmembrane potentials secondary to extracellular fields. In *Electroanaesthesia: Biomedical and Biophysical Studies*, ed. A Sances Jr, SJ Larson, pp. 176–200. New York: Academic
47. Rattay F. 1998. Analysis of the electrical excitation of CNS neurons. *IEEE Trans. Biomed. Eng.* 45:766–72
48. McIntyre CC, Grill WM. 1999. Excitation of central nervous system neurons by nonuniform electric fields. *Biophys. J.* 76:878–88
49. Rothwell J, Burke D, Hicks R, Stephen J, Woodforth I, Crawford M. 1994. Transcranial electrical stimulation of the motor cortex in man: further evidence for the site of activation. *J. Physiol.* 481:243–50
50. Day BL, Thompson PD, Dick JP, Nakashima K, Marsden CD. 1987. Different sites of action of electrical and magnetic stimulation of the human brain. *Neurosci. Lett.* 75:101–6
51. Edgley SA, Eyre JA, Lemon RN, Miller S. 1990. Excitation of the corticospinal tract by electromagnetic and electrical stimulation of the scalp in the macaque monkey. *J. Physiol.* 425:301-20
52. Henriquez CS. 1993. Simulating the electrical behavior of cardiac tissue using the bidomain model. *Crit. Rev. Biomed. Eng.* 21:1–77
53. Roth BJ. 1997. Electrical conductivity values used with the bidomain model of cardiac tissue. *IEEE Trans. Biomed. Eng.* 44: 326–28
54. Sepulveda NG, Roth BJ, Wikswo JP Jr. 1989. Current injection into a two-dimensional anisotropic bidomain. *Biophys. J.* 55:987–99
55. Roth BJ. 1992. How the anisotropy of the intracellular and extracellular conductivities influences stimulation of cardiac muscle. *J. Math. Biol.* 30:633–46
56. Knisley SB. 1995. Transmembrane voltage changes during unipolar stimulation of rabbit ventricle. *Circ. Res.* 77:1229–39
57. Neunlist M, Tung L. 1995. Spatial distribution of cardiac transmembrane potentials around an extracellular electrode: dependence on fiber orientation. *Biophys. J.* 68:2310–22
58. Wikswo JP Jr, Lin SF, Abbas RA. 1995. Virtual electrodes in cardiac tissue: a common mechanism for anodal and cathodal stimulation. *Biophys. J.* 69:2195–210
59. Roth BJ. 1995. A mathematical model of make and break electrical stimulation of cardiac tissue by a unipolar anode or cathode. *IEEE Trans. Biomed. Eng.* 42:1174-84
60. Dekker E. 1970. Direct current make and break thresholds for pacemaker electrodes on the canine ventricle. *Circ. Res.* 27:811-23
61. Hodgkin AL, Huxley AF. 1952. A quantitative description of membrane current and

its application to conduction and excitation in nerve. *J. Physiol.* 117:500–44
62. Ebihara L, Johnson EA. 1980. Fast sodium current in cardiac muscle. *Biophys. J.* 32:779–90
63. Ranjan R, Chiamvimonvat N, Thakor NV, Tomaselli GF, Marban E. 1998. Mechanism of anode break stimulation in the heart. *Biophys. J.* 74:1850–63
64. Roth BJ. 1996. Strength-interval curves for cardiac tissue predicted using the bidomain model. *J. Cardiovasc. Electrophysiol.* 7:722–37
65. Roth BJ. 1997. Nonsustained reentry following successive stimulation of cardiac tissue through a unipolar electrode. *J. Cardiovasc. Electrophysiol.* 8:768-78
66. Lin SF, Roth BJ, Wikswo JP Jr. 1999. Quatrefoil reentry in myocardium: an optical imaging study of the induction mechanism. *J. Cardiovasc. Electrophysiol.* 10:574–86
67. Efimov IR, Cheng Y, Van Wagoner DR, Mazgalev T, Tchou PJ. 1998. Virtual electrode-induced phase singularity; a basic mechanism of defibrillation failure. *Circ. Res.* 82:918–25
68. Skouibine KB, Trayanova NA, Moore PK. 1999. Anode/cathode make and break phenomena in a model of defibrillation. *IEEE Trans. Biomed. Eng.* 46:769–77
69. Roth BJ, Krassowska W. 1998. The induction of reentry in cardiac tissue. *CHAOS* 8:204–20
69a. Fischler MG. 1998. Syncytial heterogeneity as a mechanism underlying cardiac farfield stimulation during defibrillation-level shock. *J. Cardiovasc. Electrophysiol.* 9:384–94
70. Frazier DW, Krassowska W, Chen PS, Wolf PD, Dixon EG, et al. 1988. Extracellular field required for excitation in three-dimensional anisotropic canine myocardium. *Circ. Res.* 63:147–64
71. Plonsey R, Barr RC. 1986. Inclusion of junction elements in a linear cardiac model through secondary sources: application to defibrillation. *Med. Biol. Eng. Comput.* 24:137–44
72. Plonsey R, Barr RC. 1986. Effect of microscopic and macroscopic discontinuities on the response of cardiac tissue to defibrillating (stimulating) currents. *Med. Biol. Eng. Comput.* 24:130–36
73. Krassowska W, Pilkington TC, Ideker RE. 1987. Periodic conductivity as a mechanism for cardiac stimulation and defibrillation. *IEEE Trans. Biomed. Eng.* 34:555-60. Erratum. 1987. *IEEE Trans. Biomed. Eng.* 34:835
74. Fishler MG. 1997. The transient far-field response of a discontinuous one-dimensional cardiac fiber to subthreshold stimuli. *IEEE Trans. Biomed. Eng.* 44:10-18
75. Zhou XH, Ideker RE, Blitchington TF, Smith WM, Knisley SB. 1995. Optical transmembrane potential measurements during defibrillation—strength shocks in perfused rabbit hearts. *Circ. Res.* 77:593-602
76. Zhou XH, Knisley SB, Smith WM, Rollins D, Pollard AE, Ideker RE. 1998. Spatial changes in the transmembrane potential during extracellular electric stimulation. *Circ. Res.* 83:1003–14
77. Gillis AM, Fast VG, Rohr S, Kleber AG. 1996. Spatial changes in transmembrane potential during extracellular electrtical shocks in cultured monolayers of neonatal rat ventricular myocytes. *Circ. Res.* 79: 676–90
78. Trayanova NA, Roth BJ, Malden LJ. 1993. The response of a spherical heart to a uniform electric field: a bidomain analysis of cardiac stimulation. *IEEE Trans. Biomed. Eng.* 40:899–908
79. Entcheva E, Trayanova NA, Claydon FJ. 1999. Patterns of and mechanisms for shock-induced polarization in the heart: a bidomain analysis. *IEEE Trans. Biomed. Eng.* 46:260–70
80. Sobie EA, Susil RC, Tung L. 1997. A

generalized activating function for predicting virtual electrodes in cardiac tissue. *Biophys. J.* 73:1410–23

81. Entcheva E, Eason J, Efimov IR, Cheng Y, Malkin R, Claydon F. 1998. Virtual electrode effects in transvenous defibrillation-modulation by structure and interface: evidence from bidomain simulations and optical mapping. *J. Cardiovasc. Electrophysiol.* 9:949–61
82. Knisley SB, Trayanova N, Aguel F. 1999. Roles of electric field and fiber structure in cardiac electric stimulation. *Biophys. J.* 77:1404–17